RSC Advances

PAPER

View Article Online
View Journal | View Issue

Cite this: *RSC Adv.*, 2021, **11**, 11011

A novel molecularly imprinted electrochemiluminescence sensor based on cobalt nitride nanoarray electrode for the sensitive detection of bisphenol S†

Rongqi Cheng,[a] Yulong Ding,[b] Yaoguang Wang,[c] Huan Wang,[a] Yong Zhang *[a] and Qin Wei *[a]

A substitute for bisphenol A (BPA), bisphenol S (BPS) has endocrine disruptive and toxic effects and could pose potential risk on human health and the environment. Herein, we fabricated a sensitive molecularly imprinted electrochemiluminescence (MIECL) sensor for the determination of BPS. CoN nanoarray with outstanding electrical conductivity was prepared and it directly served as the sensor platform. Especially, due to the high surface area of the porous CoN nanoarray, the ECL probe of $Ru(bpy)_3^{2+}$ could be absorbed on the electrode. By means of the cation exchange of Nafion membrane and utilizing tripropylamine (TPrA) as co-reactant, boosted ECL signals were obtained. Meanwhile, by combining with molecularly imprinted polymers (MIPs), the constructed sensor achieved specific recognition of BPS. On the basis of the superior properties of the CoN nanoarray-based electrode, the ECL signal of the proposed sensor was linearly proportional to the BPS concentration from 2.4×10^{-9} to 5.0×10^{-5} mol L^{-1} ($R^2 = 0.9965$) with a low limit of detection (LOD) of 8.1×10^{-10} mol L^{-1} (S/N = 3). To test the accuracy of the proposed method, the HPLC method was adopted to analyze drinking water samples as a comparison. The *t*-test result proved that discrepancies between HPLC analysis and the method using the fabricated MIECL sensor were acceptable. The developed MIECL sensor with the sensitive, selective, reproducible, and stable analytical performance provides a potential pathway for the detection of BPS and other BPA substitutes in drinking water samples.

Received 20th December 2020
Accepted 26th February 2021

DOI: 10.1039/d0ra10676c

rsc.li/rsc-advances

1. Introduction

For the purpose of food safety and environmental protection, the use of bisphenol A (BPA) is strictly limited by the European Union and China. Currently, in response to this restriction, bisphenol S (BPS) with high thermal stability and low biodegradability has been introduced as a BPA substitute.[1] Recently, BPS has frequently been found in drinking water samples, which are filled in some "BPA-free" plastic bottles.[2,3] However, several studies have demonstrated that BPS exerts detrimental effects such as toxic and endocrine disruptive effects.[4,5] Therefore, to reduce the potential risk to human health and natural environment, the development of a simple and rapid analytical method for sensing BPS either in everyday life or in routine testing may be greatly helpful and meaningful.

So far, the determination of BPS has been achieved by following analytical methods: electrochemical sensor,[6] high performance liquid chromatography,[7] as well as gas chromatography.[8] Nevertheless, developed techniques suffer from some inevitable disadvantages, such as complicated pretreatments, low-reproducibility preparations and time-consuming operations, which greatly hinder their practical application.[9] Thus, exploring a simple, fast and reproducible electroanalytical method is necessary for the detection of BPS.

Electrochemiluminescence (ECL) assay catches great attention among the electroanalytical techniques because of its remarkable superiorities including high sensitivity, simplified equipment, and low background signals. On this basis, ECL sensors have been used successfully for bioassays in various analytical fields.[10,11] As a typical and extremely important ECL reagent, $Ru(bpy)_3^{2+}$ has been extensively applied in constructing ECL sensors for performing ultrasensitive detection of various analytes.[12,13] Nonetheless, to avoid the leak or dissolution of

[a]*Collaborative Innovation Center for Green Chemical Manufacturing and Accurate Detection, Key Laboratory of Interfacial Reaction & Sensing Analysis in Universities of Shandong, School of Chemistry and Chemical Engineering, University of Jinan, Jinan 250022, China. E-mail: Yongzhang7805@126.com*

[b]*Shanghai Quality Supervision and Inspection Technology Research Institute, Shanghai 200233, China*

[c]*Shandong Provincial Key Laboratory of Molecular Engineering, School of Chemistry and Chemical Engineering, Qilu University of Technology (Shandong Academy of Sciences), Jinan 250353, PR China*

† Electronic supplementary information (ESI) available. See DOI: 10.1039/d0ra10676c

$Ru(bpy)_3^{2+}$ from the electrode during the detection, stably immobilizing $Ru(bpy)_3^{2+}$ onto the electrode is an important challenge. Nafion, a cation exchange membrane featuring high ion-exchange selectivity, high chemical stability, and great biocompatibility, has been employed for the immobilization of $Ru(bpy)_3^{2+}$.[14] However, the modified electrode conductivity is easily affected by the Nafion membrane.[15] For obtaining the highest ECL signals and thus reducing the background noise, it is important to load as much amount of $Ru(bpy)_3^{2+}$ as possible onto the electrode; it is thus expected that a powerful approach has to be introduced to address the problems.

In order to solve this situation, several materials including nano-silica (nano-SiO_2),[16] multi-walled carbon nanotubes (MWCNTs)[17] and graphene[18] have been adopted for the construction of $Ru(bpy)_3^{2+}$-Nafion-based ECL sensors to increase the amount of the loaded $Ru(bpy)_3^{2+}$, to prevent the leak of $Ru(bpy)_3^{2+}$, and to further promote the ECL sensor performance. It is worth noting that transition metal nitrides (MNs) have emerged as novel electrode materials for sensing applications.[19] Among the reported MNs, cobalt nitride (CoN) nanoarray has attracted widespread interest, for the reason that it possesses high electronic conductivity, large specific surface areas, favorable catalytic activity, excellent chemical stability and desirable corrosion resistance.[20] More importantly, the well-designed electrode structures or elaborate electrode interfaces have significant effects on the ECL sensor performance.[21] Nanoarray electrode is a kind of artificially assembled nanostructure system. During recent years, taking advantage of the unique properties of high conductivity, large specific surface areas, close contact with the substrate,[22] high mass transfer rate, operational flexibility and favorable measurement sensitivity of a nanoarray electrode, Xie and colleagues constructed a electrochemical sensor for glucose and H_2O_2 detection with cobalt nitride array on Ti mesh as the catalyst electrode.[23] A porous cobalt nitride nanoarray grown on carbon cloth (CC) as a bifunctional electrocatalyst was successfully fabricated for overall water decomposition.[24] Thus, more attention should be paid to utilizing CoN nanoarray electrodes as excellent supporter platform candidates in the field of ECL sensors considering their large surface areas, high electronic conductivity and preparation simplicity.

Molecularly imprinted polymers (MIPs) could form complementary imprinting cavities to the template in shape, size, and functional groups in the presence of a target molecule during their synthesis process. A MIP film modified on the electrode surface serves as a molecular recognition element with its unique specific ability, which promotes the selectivity of the sensor.[25] MIPs have been introduced for chemical/biological recognition[26] owing to their desirable stability, high selectivity, excellent durability and simplicity.[27] Notably, MIPs offer numerous advantages in the preparation of electroanalytical chemical sensors, such as simple preparation process, controllable thickness of MIP film, and uniform polymer distribution on the electrode surface.[28] Based on this, a MIECL sensor equipped with the combing merits of high sensitivity, specificity, reusability, stability, automation at low cost and ease of miniaturization has achieved the detection of different targets.[29,30] To date, focus has been given to improve the MIECL sensor performance by using nanocomposite materials. Lin *et al.* developed a new MIP-ECL sensor based on MWCNTs/nano-TiO_2 nanocomposite for BPA detection.[31] Necip Atar *et al.* proposed a MIECL sensor of atrazine by employing Pt nanoparticle/C_3N_4 nanotube nanocomposites as the sensor carrier.[32] Bahareh Babamiri *et al.* reported a MIECL sensor which used GO–Fe_3O_4 composites as the sensing platform for the detection of creatinine.[33] However, difficulties still remain in the further development of the MIECL sensor. The cumbersome electrode assembly process in the preparation of these published MIECL sensors showed detrimental effects on cost, reproducibility, and mass-scale application of the sensor. In view of the above, a MIECL sensor based on CoN nanoarray electrode serving as a novel sensing platform is a good alternative to monitor BPS by virtue of its low cost, high selectivity, great reproducibility and desirable sensitivity. As far as we know, CoN nanoarray electrodes have not been studied and reported in the application of preparing MIECL sensors.

In this work, a novel MIECL sensor was designed for the sensitive and selective determination of BPS. As shown in Scheme 1(A), CoN nanoarray grown directly on a carbon cloth (CC) electrode was firstly prepared by hydrothermal methods and *in situ* conversion, which served as a nanoarray electrode. As shown in Scheme 1(B), Nafion was used for immobilizing luminophores $Ru(bpy)_3^{2+}$ *via* the cation exchange. By virtue of its unique properties of large surface areas and superior electrical conductivity, CoN nanoarray electrode tremendously supported a large amount of luminophores $Ru(bpy)_3^{2+}$, which could emit a stronger ECL signal. Besides, due to the MIPs modified on the CoN nanoarrays loaded with $Ru(bpy)_3^{2+}$-Nafion, stable and accurate ECL signals were obtained. Then, in the presence of the template molecules BPS, the ECL response of the sensor gradually reduced with increasing BPS concentration. Based on the elution and adsorption of the template molecules in MIPs, the template BPS was specifically recognized, and the MIECL sensor was endowed with good selectivity to achieve the quantitative determination of BPS. Eventually,

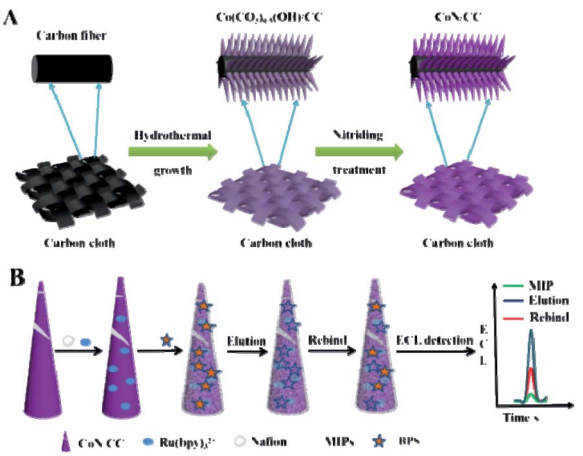

Scheme 1 Schematic of (A) the preparation process of CoN/CC and (B) fabrication procedure of the MIECL sensor.

the constructed MIECL sensor received a satisfactory analytical feedback for the determination of BPS in drinking water samples.

2. Experimental

2.1 Chemicals and apparatus

Cobalt nitrate (98%), 2-methacrylic acid (MAA, 99%), ammonium fluoride (95%), ethylene glycol dimethacrylate (EDMA, 98%), acetonitrile (AR), BPS and azobisisobutylnitrile (AIBN, 98%) were supplied by Macklin (Shanghai, China). In addition, tris(2,2-bipyridyl)dichlororuthenium(II) hexahydrate ($Ru(bpy)_3Cl_2 \cdot 6H_2O$), urea (99%), potassium ferricyanide ($K_3[Fe(CN)_6]$), potassium ferrocyanide ($K_3[Fe(CN)_6]$), potassium chloride (KCl) and potassium nitrate (KNO_3) were purchased from Sinopharm (Beijing, China). All the reagents used in the experiment were analytical grade reagents, and ultrapure water (18.25 MΩ cm^{-1}) was used throughout the experiments.

The microstructure of the products was observed by scanning electron microscopy (SEM, JSM250F) and transmission electron microscopy (TEM, JEOL JEM-2100F). The X-ray diffraction (XRD) pattern was measured by the D8 focus diffractometer (Bruker AXS, Germany). The XPS analysis was performed on the Thermo ESCALAB 250XI system. The electrochemiluminescence measurements were carried out on the model MPI-F flow injection chemiluminescence detector (Remax, China). The RST 5000 electrochemical work station (Suzhou Ruisite Instrument Co, Ltd) was applied to accomplish the electrochemical impedance spectroscopy (EIS) measurements. The tube furnace that we used was acquired from Zhong yi guo ke (Beijing, China).

2.2 Preparation of CoN/CC

Commercial CC (3 cm × 2 cm) was hydrothermally pretreated in a 10% nitric acid solution at 120 °C for 2 h to enhance the hydrophilicity at first. Afterward, the pretreated CC (3 cm × 2 cm) was washed with ultrasonic water, and placed in a beaker containing ethanol for the subsequent experiments. For the preparation of the CoN/CC, 2 mmol of cobalt nitrate, 6 mmol of urea and 4 mmol of ammonium fluoride were firstly dissolved in 30 mL distilled water under magnetic stirring to achieve a homogeneous solution. Then, the mixed amaranthine solution was poured into a 50 mL Teflon-lined stainless-steel autoclave. Subsequently, the pretreated CC (3 cm × 2 cm) was vertically placed into the solution in the autoclave, following which it was reacted at 120 °C for 6 h. After the autoclave cooled to ambient temperature, the cobalt hydroxide nanoarray grown on CC was rinsed with ultrasonic water. The cobalt hydroxide nanoarray precursor was obtained, following which it was dried in a vacuum oven overnight at 60 °C. At last, the well-prepared cobalt hydroxide nanoarray precursor was in-site converted to CoN nanoarray following the nitride process. Specifically, after purging with argon gas (Ar) for 15 min in a tubular furnace, the obtained cobalt hydroxide nanoarray precursor was placed into a clean porcelain boat and then the boat was moved to the middle of the tubular furnace. The nitride reaction was performed in ammonia gas in the tube furnace at 380 °C for 3 h at a heating rate of 5 °C min^{-1}. After cooling down to room temperature with the protection of Ar gas, CoN/CC was prepared.

2.3 Preparation of MIP and non-imprinted polymer (NIP) precursor solution

The MIP precursor solution was prepared by bulk polymerization method. Firstly, 0.008 mmol of BPS as template molecule and 0.4 mmol of 2-methacrylic acid (MAA) as functional monomer were added into a beaker to dissolve ultrasonically. Next, the above solution mixture was magnetically stirred to dissolve by the addition of 10 mmol of ethylene glycol dimethacrylate (EDMA) as cross-linking agent and 1 mmol of azobisisobutylnitrile (AIBN) as initiator. Finally, the obtained transform solution used as MIP precursor solution was protected under N_2 atmosphere. The NIP precursor solution was prepared by the same process as that of preparing the MIP precursor solution in the absence of BPS.

2.4 Preparation of the MIECL sensor

As illustrated in Scheme 1(B), 6 μL of Nafion was firstly coated on the prepared CoN/CC electrode surface (0.5 cm × 0.5 cm) and dried in air. Then, the above modified electrode was soaked in 5 mmol L^{-1} $Ru(bpy)_3^{2+}$ solution for 30 min incubation and naturally dried to form the light-emitting layer on the electrode (named as $Ru(bpy)_3^{2+}$/Nafion/CoN/CC electrode). After that, the decorated electrode (named as MIP/$Ru(bpy)_3^{2+}$/Nafion/CoN/CC electrode) was acquired by immersing into the prepared MIP precursor solution for 6 min incubation. The above obtained electrode was immersed in methanol/acetic acid (9 : 1, v/v) solution with gentle stirring for 10 min to remove the BPS template after the electrode was dried in the air. Finally, the resulting electrode was subsequently washed with water and allowed to dry naturally (denoted as eluted MIP/$Ru(bpy)_3^{2+}$/Nafion/CoN/CC electrode), which was the MIECL sensor preserved for further use. The non-imprinted electrochemiluminescence (NIECL) sensor was prepared in light of the same procedure as above except for replacing the NIP precursor solution for the MIP precursor solution.

2.5 Electrochemical and ECL measurement

MPI-F ECL analyzer and electrochemical impedance spectroscopy (EIS) were applied for the ECL and electrochemical measurements, respectively. A three-electrode system was established for recording the ECL response, including the prepared CoN nanoarray electrode as the working electrode, platinum as the counter electrode, and Ag/AgCl as the reference electrode. With regard to the ECL test, the electrode was immersed in 10 mL of 0.1 mol L^{-1} PBS (pH = 7.4) containing 55 mmol L^{-1} of TPrA as co-reactant at room temperature and the voltage of the photomultiplier tube (PMT) was set at 800 V with the scan potential range from 0.0 V to 1.5 V. The EIS detection was conducted in a solution containing 2.5 mmol L^{-1} $K_3[Fe(CN)_6]/K_4[Fe(CN)_6]$ and 0.1 mmol L^{-1} KCl. The frequency range was set between 100 mHz and 100 kHz.

3. Results and discussion

3.1 Morphology and structure characterization of the MIECL sensor

The morphology of the CoN precursor, CoN/CC, MIP/Ru(bpy)$_3^{2+}$/Nafion/CoN/CC, and NIP/Ru(bpy)$_3^{2+}$/Nafion/CoN/CC were, respectively, characterized by a scanning electron microscope (SEM). As presented in Fig. 1A, the CoN precursor presented a needle-like nanoarray morphology. As shown in Fig. 1B, the overall structure of the needle-like nanoarray remained unchanged after the ammonia nitride transformation. An evenly covered MIP film on the modified electrode can be found in Fig. 1C. Fig. 1D displays that the NIP membrane was also distributed on the modified electrode surface uniformly. The morphology of MIP/Ru(bpy)$_3^{2+}$/Nafion/CoN/CC before elution and NIP/Ru(bpy)$_3^{2+}$/Nafion/CoN/CC before elution showed no difference. The detailed structure of CoN/CC was confirmed by transmission electron microscopy (TEM) analysis. The porous structure of CoN/CC was observed as exhibited in Fig. 1E and F.

The X-ray diffraction (XRD) spectrum was employed for analyzing the phase composition of the samples. As shown in Fig. 2A, four diffraction peaks appeared, corresponding to the (111), (200), (220), and (311) crystal phase reflection of CoN (JCPDS 16-0116). To validate the surface elemental composition and the valence states of the CoN nanoarrays, the X-ray photoelectron spectroscopy (XPS) test was conducted. As displayed in Fig. 2B, the characteristic diffraction peaks located at 284.8 eV, 399.4 eV, 529.7 eV, and 780.6 eV were attributed to C 1s, N 1s, O 1s, and Co 2p, respectively. Furthermore, as shown in Fig. 2C, by the deconvolution of the Co 2p spectrum of the CoN nanoarrays, two peaks appeared at 780.5 eV and 787.1 eV and were indexed to the spin–orbit splitting values of Co $2p_{3/2}$. The two peaks at 796.6 eV and 802.9 eV were ascribed to the spin–orbit splitting values of Co $2p_{1/2}$. Moreover, the peaks centered at 780.5 eV and 796.6 eV were assigned to Co(III) and the two peaks at 787.1 eV and 802.9 eV corresponded to Co(II).[34] The results

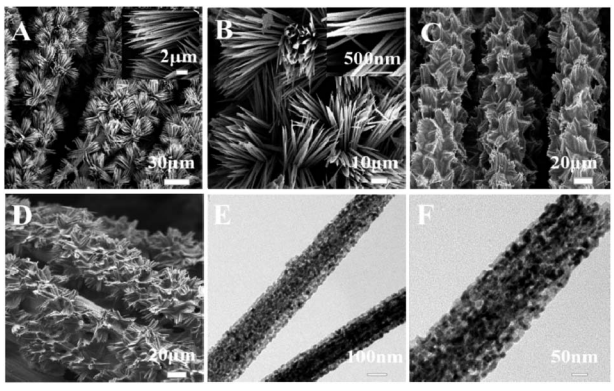

Fig. 1 (A) SEM images of CoN precursor, (B) CoN/CC (the inset displaying the corresponding SEM image at high magnification), (C) MIP/Ru(bpy)$_3^{2+}$/Nafion/CoN/CC before elution, (D) NIP/Ru(bpy)$_3^{2+}$/Nafion/CoN/CC before elution, (E) low-magnification TEM image of CoN/CC, (F) high-magnification TEM image of CoN/CC.

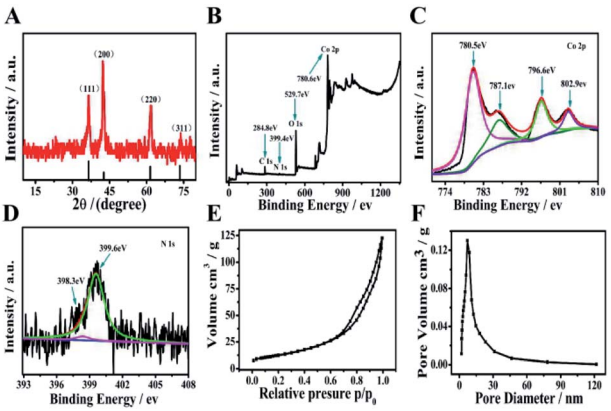

Fig. 2 (A) XRD patterns of CoN nanoarrays, (B) wide-scan XPS spectrum of CoN nanoarrays, (C) XPS spectrum of the deconvoluted Co 2p of CoN nanoarrays, (D) XPS spectrum of the deconvoluted N 1s of CoN nanoarrays, (E) N_2 sorption isotherm curve of CoN nanoarrays, (F) BJH pore-size distribution of CoN nanoarrays.

suggested that the Co(II) species in the CoN precursor (*i.e.*, $Co(CO_3)_{0.5}(OH)\cdot xH_2O$) were converted into Co(III) species in CoN. A typical peak appeared at 780.5 eV in the Co 2p spectrum, which was ascribed to the binding energy of the Co–N bond. As illustrated in Fig. 2D, by the deconvolution of the deconvoluted N 1s spectrum of the CoN nanoarrays, two peaks centered at 399.6 eV and 398.3 eV were observed, which belonged to Co–N and pyridinic N.[35,36] The peak at 399.6 eV belonged to Co–N bonds in the N 1s spectrum, which was in good agreement with the peak located at 780.5 eV in the Co 2p spectrum. The above results indicated that the CoN nanoarrays were prepared successfully.

The nitrogen adsorption–desorption experiment at 77 K was performed to further verify the porous structure of the CoN nanoarrays. In accordance with the Brunauer–Emmett–Teller (BET) analysis, the CoN nanoarrays showed the typical IV isotherm adsorption lag characteristics as depicted in Fig. 2E, suggesting the presence of numerous mesopores in the CoN nanoarrays. Meanwhile, the rise in the adsorption ability in the curve at the lower relative pressure ($p/p_0 < 0.2$) indicated the existence of micropores. The specific surface area of the CoN nanoarrays was around 143.09 m^2 g^{-1}. The corresponding pore size distribution plots are exhibited in Fig. 2F, which were calculated from the adsorption branch of the nitrogen adsorption isotherm with the Barrett–Joyner–Halenda (BJH) method. This further demonstrated that there were no abundant mesoporous (~4.2 nm) in the CoN nanoarrays, which contributed to the exposure of the active sites and the penetration of liquid electrolytes.[37]

To further validate the successful polymerization of the BPS MIP, the Fourier transform infrared (FTIR) spectra of BPS, MAA, and BPS-MIP are given in Fig. S1A.† In curve a, the peak at around 3496 cm^{-1} suggested the presence of a hydroxyl group (–OH) in BPS. The band at about 1502 cm^{-1} corresponded to the stretching vibration of the benzene ring skeleton –C=C. The small band at about 2970 cm^{-1} represented the existence of the –C–H stretching vibration. The –C–O stretching vibration

located at around 1245 cm^{-1} was also observed. The existence of the –OH group in the spectrum of MAA (curve b) was confirmed by the broad absorption from 3500 cm^{-1} to 3700 cm^{-1}. Meanwhile, the peak at around 1723 cm^{-1} could be attributed to the carbonyl group (–C=O) in both MAA and crosslinking agent EDMA. The absorption peaks in curve c at 1154 cm^{-1}, 1257 cm^{-1}, 1458 cm^{-1} were, respectively, assigned to the symmetric vibration –C–O–, the asymmetric stretching vibration –C–O– and the bending vibration –CH_2–, respectively, in both MAA and EDMA.[38] The absorption band in the range (2800–3000 cm^{-1}) demonstrated the appearance of methyl (–CH_3) and methylene groups (–CH_2) in both MAA and crosslinking agent EDMA.[39] The carbonyl (–C=O) functional groups of MAA could interact with the hydroxy (–OH) functional groups of the template BPS through hydrogen bonds. The above results confirmed the successful synthesis of BPS-MIP.

3.2 Preparation and identification mechanism of the MIP for BPS

In the conventional bulk polymerization process, the carbonyl functional groups of MAA could build hydrogen bindings with the hydroxy functional groups of the template BPS. EDMA, which possesses two allyl groups, is utilized as the crosslinking agent to control the stability of the imprinted cavity and the flexibility of the polymer matrix.[40] The eluent methanol/acetic acid (9 : 1, v/v) solution removes the template molecule BPS by breaking the hydrogen bonds between MAA and BPS. The elution of the target molecules BPS on the MIP film leaves the imprinted binding cavities complementary in size and shape to the template BPS. These imprinted binding sites could specifically recognize the template molecule BPS through hydrogen bond interaction and shape, size identification.

3.3 Electrochemical characterization of the MIECL sensor

The stepwise procedure for the characterization of the MIECL sensor was *via* the EIS method. EIS Nyquist plots were composed of a high-frequency semicircular portion corresponding to the limited process of electron transfer and a low-frequency linear part relating to the diffusion-controlled process. The diameter of the semicircle corresponds to the electron transfer resistance (R_{et}), which indicates the changes in the electrode–solution interface.[41] As illustrated in Fig. 3A, a small semicircle appeared for CoN/CC (curve a), manifesting that the CoN/CC electrode exhibited an extraordinary conductivity as well as a high enlarged specific surface area. When the MIP film was covered on the surface of $Ru(bpy)_3^{2+}$/Nafion/CoN/CC, the electron transfer resistance value (curve d) significantly increased by reason of the restriction of a dense non-conductive film. Whereas the corresponding resistances (curve b) diminished dramatically after the extraction of the template molecules, denoting that the cavities exposed as electron transfer channels could facilitate the $[Fe(CN_6)]^{3-/4-}$ probe to the electrode surface. Subsequently, conspicuous enhancements in impedance values were observed again (curve c) after rebinding with 1.0×10^{-6} mol L^{-1} BPS. The reason was that most of the empty binding cavities masked by the template molecules made

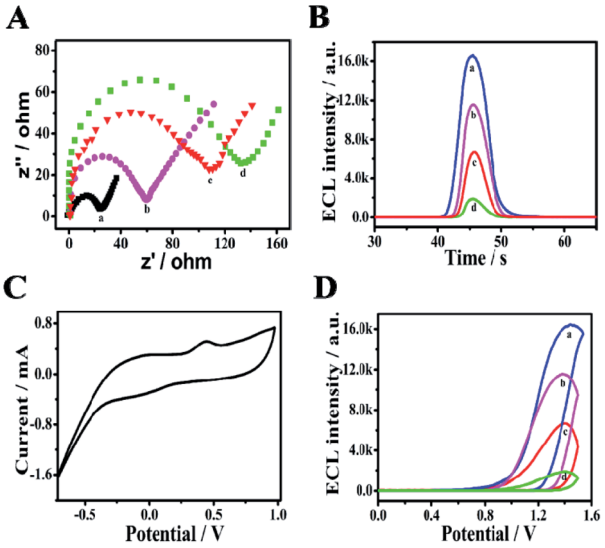

Fig. 3 (A) EIS responses of stepwise-assembled electrodes: (a) CoN/CC, (b) eluted MIP/$Ru(bpy)_3^{2+}$/Nafion/CoN/CC, (c) rebinding MIP/$Ru(bpy)_3^{2+}$/Nafion/CoN/CC, (d) MIP/$Ru(bpy)_3^{2+}$/Nafion/CoN/CC in a solution containing 2.5 mmol L^{-1} $K_3[Fe(CN)_6]/K_4[Fe(CN)_6]$ and 0.1 mmol L^{-1} KCl; (B) ECL profiles of each electrode modification step in 10 mL of 0.1 mol L^{-1} PBS (pH 7.4) containing 55 mmol L^{-1} of TPrA: (a) $Ru(bpy)_3^{2+}$/Nafion/CoN/CC, (b) eluted MIP/$Ru(bpy)_3^{2+}$/Nafion/CoN/CC, (c) rebinding MIP/$Ru(bpy)_3^{2+}$/Nafion/CoN/CC, (d) MIP/$Ru(bpy)_3^{2+}$/Nafion/CoN/CC; (C) CV curves of 0.1 mol L^{-1} BPS in 0.1 mol L^{-1} PBS (pH 7.4), (D) ECL intensity–potential curves of (a) $Ru(bpy)_3^{2+}$/Nafion/CoN/CC, (b) eluted MIP/$Ru(bpy)_3^{2+}$/Nafion/CoN/CC, (c) rebinding MIP/$Ru(bpy)_3^{2+}$/Nafion/CoN/CC, (d) MIP/$Ru(bpy)_3^{2+}$/Nafion/CoN/CC in 10 mL of 0.1 mol L^{-1} PBS (pH 7.4) containing 55 mmol L^{-1} of TPrA.

the electron transport much harder. These impedance changes confirmed the successful construction of the proposed MIECL sensor.

The cyclic voltammetry characterizations of various electrodes were investigated (Fig. S1B†). It was observed that there was a pair of reduction–oxidation peaks on the bare CC electrode (curve a). Following the CC electrode surface modification by Nafion-$Ru(bpy)_3^{2+}$, the redox peaks nearly disappeared (curve b), which was due to the fact that the one-electron redox reaction of $Fe(CN)_6^{3-/4-}$ was inhibited by the Nafion film.[42] The remarkable enhancements in the redox peak currents were observed (curve c) after the introduction of the CoN/CC electrode, revealing that the excellent electrical conductivity of the CoN/CC electrode was conducive to accelerate the electron transfer process.

3.4 ECL characterization of the MIECL sensor

The obvious differences in the ECL response during the assembly process of the constructed sensor were investigated. As shown in Fig. S1C,† the ECL intensity of $Ru(bpy)_3^{2+}$/Nafion/CoN/CC (curve f) was much stronger than that of $Ru(bpy)_3^{2+}$/Nafion/CC (curve e), which could be attributed to the CoN nanoarray as supporter with a predominant conductive property and a large surface area. Simultaneously, as presented in Fig. 3B, the ECL response was further amplified (curve a) since

the luminophore $Ru(bpy)_3^{2+}$ was loaded on the electrode by the cation exchange of the Nafion membrane and the luminophore $Ru(bpy)_3^{2+}$ could be absorbed on the porous CoN nanoarray electrode with a large surface area and superior conductivity. The ECL emission descended sharply (curve d) after the introduction of the MIP film, indicating the direct hindrance of the electron transfer between the co-reactant TPrA and $Ru(bpy)_3^{2+}$. Furthermore, on account of the generation of recognition sites, the ECL value was elevated (curve b). Afterwards, the template molecules rebound with the MIP pores because the similarity in size and shape to holes prevented the co-reactant TPrA from accessing the electrode surface, and, eventually, the ECL intensity reduced again (curve c). As a comparison, the ECL emission of the NIP/$Ru(bpy)_3^{2+}$/Nafion/CoN/CC electrode (curve g) in Fig. S1D† was higher than that of the MIP/$Ru(bpy)_3^{2+}$/Nafion/CoN/CC electrode (curve d) in Fig. 3B. A slight ECL intensity change of the eluted NIP/$Ru(bpy)_3^{2+}$/Nafion/CoN/CC electrode (curve h) is also observed in Fig. S1D,† which was due to the fact that specific recognition sites were absent on the eluted NIP/$Ru(bpy)_3^{2+}$/Nafion/CoN/CC electrode surface. Additionally, the ECL response of the NIECL sensor after rebinding the template BPS (curve i) slightly reduced owing to the lack of specific imprinted binding sites in the NIECL sensor. The above results further indicated that the proposed MIECL sensor exhibited a favorable specific recognition capability towards BPS.

3.5 The sensing mechanism of the MIECL sensor

The possible mechanism of the proposed MIECL sensor during ECL electron transfer was discussed. The co-reactant TPrA was electrooxidized to $TPrA^{\bullet+}$ and meanwhile $Ru(bpy)_3^{2+}$ was oxidized to $Ru(bpy)_3^{3+}$. Then, the short-life $TPrA^{\bullet+}$ was protonated to form $TPrA^{\bullet}$ intermediate, producing an excited state $Ru(bpy)_3^{2+}$* through the procedure of electron transfer. Afterwards, the unstable $Ru(bpy)_3^{2+}$* was returned to the ground state $Ru(bpy)_3^{2+}$ releasing the photons to generate a stronger electrode. However, the ECL behavior was effectively restrained in this system after the introduction of BPS. Fig. S3A† presents two UV absorption peaks at 225 nm and 274 nm (curve a), which belonged to individual BPS. As depicted in Fig. S3A,† the UV absorption band of individual $Ru(bpy)_3^{2+}$ appeared at 285 nm and 453 nm, corresponding to the π–π* transition and metal-to-ligand charge transfer of $Ru(bpy)_3^{2+}$ (curve b), respectively. However, in the case of the coexistence of BPS and $Ru(bpy)_3^{2+}$, the adsorption peaks of the mixture were exactly the merging of their individual ones (curve c), indicating that the two species can't directly react with each other. Similarly, it was found (Fig. S3B†) that no direct chemical reaction between BPS and TPrA can be expected. Besides, Fig. S3C† exhibits that the adsorption bands of the $Ru(bpy)_3^{2+}$/TPrA/BPS mixture (curve c) were exactly the sums of the individual ones (curve a, curve b), illustrating that these species can't react with each other. The irreversible electro-oxidation peak of BPS at 0.45 V was observed in the cyclic voltammetry curve (Fig. 3C), which was much lower than that of $Ru(bpy)_3^{2+}$. As a consequence, it could be inferred that their inhibition capacity could be originated from the oxidation product of BPS. Similar to previous reports,[43,44] the ECL quenching mechanism might be ascribed to the electron transfer process between the excited state $Ru(bpy)_3^{2+}$* and the BPS oxidation product. In this reaction process, the electrons of $Ru(bpy)_3^{2+}$* were moved to the BPS oxidation product and $Ru(bpy)_3^{2+}$* decayed to $Ru(bpy)_3^{2+}$ to achieve ECL emission. Then, the reduced ECL response was obtained.

In order to further clarify this process, the corresponding ECL potential responses were recorded (Fig. 3D). The $Ru(bpy)_3^{2+}$ was modified on the CoN nanoarray electrode, and a stronger ECL emission (curve a) was generated at 1.39 V in the presence of TPrA. The remarkable decrease in the ECL response (curve d) could be explained by the formed nonconductive MIP membrane blocking TPrA from reaching the electrode surface. However, the ECL signal enhancements were observed again (curve b) after washing the MIP layer with methanol/acetic acid (9 : 1 in volume), originating from the TPrA entering the molecularly imprinted cavities acting as the electron transfer tunnels. Subsequently, the ECL response declined again (curve c) with the formation of a compact non-conducting polymer film, and, meanwhile, the target BPS played a crucial role in inhibiting the luminous efficiency of $Ru(bpy)_3^{2+}$. Apparently, the ECL value after rebinding with the template molecules (curve c) was lower compared with the ECL intensity in the absence of BPS (curve b). The reason behind this might be that the majority of the cavities were occupied by the template molecules, which suppressed electron transportation. Given the ECL value change, the use of the MIECL sensor will be a promising analysis method candidate for detecting BPS.

3.6 Optimization of experimental conditions

For the purpose of fulfilling the best performance of the MIECL sensor, the effects of experimental conditions such as the pH value of PBS, the concentration of $Ru(bpy)_3^{2+}$, the concentration of TPrA, the molar ratio of template to monomer, and the incubation time of MIP were optimized. The effect of pH on the ECL intensity was evaluated in 10 mL of 0.1 mol L^{-1} PBS containing 55 mmol L^{-1} of TPrA. As depicted in Fig. S2A,† when the pH of the test solution was 7.4, the ECL response reached the peak value. In this case, the experimental result demonstrated that pH 7.4 was favorable. The ECL signal was recorded in the $Ru(bpy)_3^{2+}$ concentration range of 2–7 mmol L^{-1} as exhibited in Fig. S2B.† The ECL signal enhanced gradually with the increase in $Ru(bpy)_3^{2+}$ concentration within 5 mmol L^{-1} and began to decrease thereafter. Even though the high concentration of $Ru(bpy)_3^{2+}$ was beneficial to promote the ECL value of the sensor, excessive amount of $Ru(bpy)_3^{2+}$ would increase the impedance in the modified layer, leading to the reduction in the emission signal. Therefore, 5 mmol L^{-1} $Ru(bpy)_3^{2+}$ was selected for the subsequent study. The optimum concentration of TPrA was investigated (Fig. S2C†) in PBS with the optimal pH value. The ECL response ascended with increasing concentration of TPrA, firstly, reached a maximum ECL value at 50 mmol L^{-1}, and then showed a distinct downward trend. As a result, the concentration of 50 mmol L^{-1} was used in the following assays.

The effect of the monomer to template ratio was investigated in this experiment. A series of MIECL sensors prepared with different ratios (50 : 1, 100 : 1, 150 : 1, 200 : 1, 300 : 1) were analyzed by rebinding with 8.0×10^{-6} mol L^{-1} of the template BPS. Fig. S2D† exhibits that the optimum ECL intensity response was obtained at a monomer/template ratio of 100. It had an adverse impact on rebinding affinity when the monomer/template ratio was lower or higher than 100. At the ratio of less than 100, the amount of the functional monomer was too inadequate to combine enough template molecules, leading to the difficulty in forming effective imprinted binding sites.[45] Nevertheless, at the ratio of higher than 100, fewer template molecules were involved in the formation of MIPs, resulting in fewer number of recognition sites in the polymer structure.[46] Therefore, the monomer/template ratio of 100 : 1 was employed for this work.

Besides, the value of appropriate incubation time (as shown in Fig. S2E†) was an indispensable factor affecting the ECL response. The prepared sensor was immersed into the BPS molecular polymer solution for 2–12 min in this experiment, and the ECL signal variation was recorded every two minutes. When the incubation time reached 8 min, the higher ECL signal occurred. As is known to all, the sensitivity of the MIECL sensor depends on the number of effective recognition sites in the MIP. The shorter the incubation time is, the thinner the MIP film will be. Consequently, there will be insufficient effective imprinting cavities with the thinner film, leading to low binding capacity. The longer the incubation time is, the thicker the imprinted membrane will be. However, too thick MIP film hinders the complete removal of template molecules. Hence, 8 min was adopted as the incubation time for further experiments. Additionally, the effect of elution time from 2 min to 12 min on the ECL intensity was studied. As can be seen in Fig. S2F,† the ECL intensity gradually enhanced with the increasing elution time varying from 2 min to 10 min, and then reached a steady value after 10 min. Thus, 10 min was selected as the optimal elution time.

3.7 Sensing performance of the MIECL sensor

After affirming the optimal conditions, the quantitative determination of BPS was conducted with the fabricated MIECL sensor. As exhibited in Fig. 4A, the ECL response (I, where I represents the obtained ECL intensity) descended gradually accompanying the increasing concentration of BPS. It can be seen (Fig. 4B) that after rebinding with BPS, the ECL response difference ΔI_{ECL} ($\Delta I_{ECL} = I_0 - I$, where I_0 stands for the original ECL intensity) exhibited a good linear relationship towards the logarithm of BPS concentration from 2.4×10^{-9} mol L^{-1} to 5.0×10^{-5} mol L^{-1}. The linear regression equation was described as ΔI_{ECL} (a.u.) = 1053.4 lg C (mol L^{-1}) + 11 510 with a correlation coefficient of 0.9965. The limit of detection (LOD) was figured to be 8.1×10^{-10} mol L^{-1} at a signal-to-noise ratio of 3. To further prove the superior sensing performance of the proposed MIECL sensor, we compared this method with the previous reports for detecting BPS. It can be clearly noticed that the proposed MIECL sensor studied in this work presented

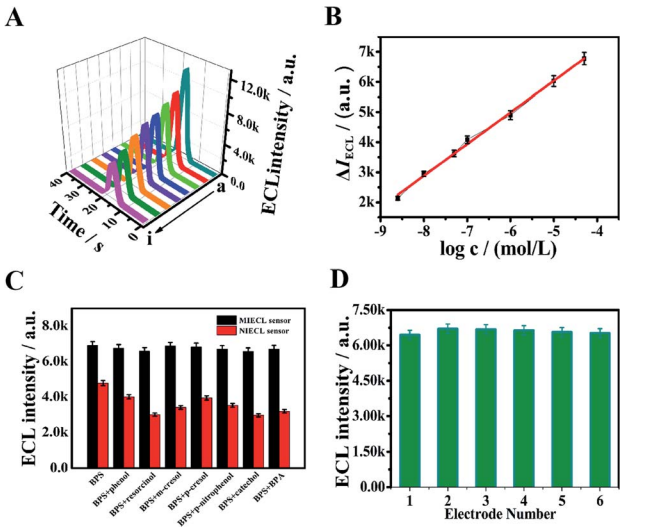

Fig. 4 (A) ECL–time curves of the MIECL sensor with different concentrations of BPS (a → i): 0, 2.4×10^{-9} mol L^{-1}, 1.0×10^{-8} mol L^{-1}, 5.0×10^{-8} mol L^{-1}, 1.0×10^{-7} mol L^{-1}, 1.0×10^{-6} mol L^{-1}, 1.0×10^{-5} mol L^{-1}, 5.0×10^{-5} mol L^{-1}, (B) calibration curves of the MIECL sensor, (C) selectivity of the MIECL sensor and the NIECL sensor, (D) reproducibility of six MIECL sensors incubated with 1.0×10^{-6} mol L^{-1} BPS.

a wider linear range and/or a lower LOD in comparison with the other published BPS detection methods (Table S1†). Due to the fact that the research on the ECL method for detecting BPS is scarce, we made a comparison between the present work and other reported ECL methods to determine BPA (BPS is used as a substitute for BPA). The corresponding comparison results listed in Table S2† suggested that the developed MIECL sensor achieved a more sensitive BPS detection. The wider linear range and/or the lower LOD of the MIECL sensor may be attributed to the CoN nanoarray electrode merits including large surface areas, a porous feature, and high electronic conductivity, which was beneficial to facilitate the electron transfer and effectively increase the active sites for binding to BPS. As for real sample testing, the broader linear range made the preparation of the sample solution more convenient.

3.8 Selectivity, reproducibility and stability of the MIECL sensor

In order to assess the selectivity of the fabricated MIECL sensor for BPS detection, the structurally similar compounds (100 folds phenol and BPA, 50 folds resorcinol, *m*-cresol, *p*-nitrophenol, and cresol) were selected as the interfering substances for specific recognition study. As presented in Fig. 4C, there was no significant ECL response change from the MIECL sensor in the mixtures containing BPS and other interfering substances compared to that of the sensor with only BPS. Meanwhile, in the coexistence of BPS and interference substances, an evident ECL signal change from the NIECL sensor was observed (Fig. 4C). The reason was the lack of selective recognition sites in the NIECL sensor. The selectivity of the proposed sensor lay in the imprinted binding sites on the MIP membrane. The target BPS

could be specifically recognized on the imprinted binding sites *via* hydrogen bonding, shape and size. Hence, the above results illustrated that the developed MIECL sensor presented satisfactory selectivity towards BPS detection.

With aim of confirming the reproducibility of the proposed sensor, the ECL intensities of six different sensors prepared under the same conditions were measured. As shown in Fig. 4D, a desirable result with a relative standard deviation (RSD) value was calculated as 2.85%. Moreover, the repeatability of the MIECL sensor was also evaluated. The ECL response of the proposed MIECL sensor was measured for a new BPS solution (1.0×10^{-6} mol L^{-1}) each time after six elution–readsorption cycles. As can be seen from Fig. S4A,† the ECL intensity exhibited a slight decline after six times of tests and the relative standard deviation (RSD) was less than 1.46%, revealing that the MIECL sensor possessed desirable repeatability for BPS detection. At the same time, the long-time stability of the MIECL sensor was investigated. The freshly prepared MIECL sensor was stored in the refrigerator at 4 °C for subsequent use. The ECL intensity of the MIECL sensor was detected in 10 mL of 0.1 mol L^{-1} PBS (pH 7.4) containing 50 mmol L^{-1} of TPrA after one week, two weeks, three weeks, and four weeks, respectively. As portrayed in Fig. S4B and C,† the ECL intensity decreased by 5.8% after two weeks. The MIECL sensor maintained over 85% of its original response value after a storage period of four weeks, meaning that our constructed MIECL sensor exhibited acceptable stability towards BPS.

3.9 Analysis of BPS in real sample

To further appraise the reliability of the proposed method in practical applications, the pretreated MIECL sensor was employed to detect BPS in drinking water samples *via* the standard addition method. The drinking water samples were obtained from a shop in the University of Jinan. To begin with, the drinking water samples were appropriately processed with 0.1 mol L^{-1} PBS (pH 7.4) buffer in accordance with a previous report.[47] Then, three drinking water samples were prepared by spiking with BPS standard solution at different concentrations (5.0×10^{-6} mol L^{-1}, 10.0×10^{-6} mol L^{-1}, 15.0×10^{-6} mol L^{-1}). Subsequently, the recovery experiments were carried out. The fabricated MIECL sensor was immersed into the resulting sample solutions for ECL signal detection and 10 mL of 0.1 mol L^{-1} PBS (pH 7.4) including 50 mmol L^{-1} of TPrA was utilized as co-reactant. The measurement of each sample was carried out in quintuplicate. With the aim of testifying the accuracy of the proposed method, the high performance liquid chromatography (HPLC) method was also adopted to analyze the drinking water samples. The corresponding detection results are listed in Table S3.† It was found that the discrepancies between the analysis using HPLC and the developed MIECL sensor were acceptable. The *t*-test was applied to compare the HPLC method with the present method. It can be seen from Table S4† that the calculated *t* value was less than 2.306 at the confidence level of 95%. The results indicated that no obvious difference between the two approaches appeared at the confidence level of 95%. Besides, the recovery range of the proposed sensor was between 98.0% and 104.6% with the RSD ranging from 2.6% to 3.3%, which proved that the fabricated sensor had a promising prospect for application in real sample analysis.

4. Conclusion

For the sensitive and rapid detection of BPS, a novel and robust MIECL sensor was constructed based on combining CoN nanoarray electrode and MIP technology. The stable ECL probe of $Ru(bpy)_3^{2+}$ was loaded on the nanoarray electrode surface through the physical adsorption of the CoN nanoarrays and cation exchange of Nafion, and the excellent anodic ECL response of $Ru(bpy)_3^{2+}$ could be obtained by virtue of the high surface areas and excellent electrical conductivity of the CoN nanoarrays. Besides, the enhancement of the ECL intensity was observed after the elution of the template molecule. Afterwards, with the introduction of the target molecules of BPS, the molecularly imprinted cavities of the eluted MIPs were occupied by the targets, resulting in an apparent decrease in ECL response. Due to the combination of the ECL behavior and the specific recognition property of MIPs, the established MIECL sensor presented outstanding characteristics such as sensitivity, stability, reproducibility, repeatability, and broad linear range within 2.4×10^{-9} mol L^{-1} to 5.0×10^{-5} mol L^{-1} with a low LOD of 8.1×10^{-10} mol L^{-1}. In this way, the obtained MIP-ECL sensor showed great promise in monitoring BPS and its analogues.

Conflicts of interest

There are no conflicts to declare.

Acknowledgements

This study was supported by the National Natural Science Foundation of China (21775053, 21777056, 22006080), the Natural Science Foundation of Shandong Province (2019GSF111023, ZR2020QB094), the National Key Scientific Instrument and Equipment Development Project of China (No. 21627809) and the Program for Scientific Research Innovation Team in Colleges and Universities of Shandong Province.

References

1 L. H. Wu, X. M. Zhang, F. Wang, C. J. Gao, D. Chen, J. R. Palumbo, Y. Guo and E. Y. Zeng, *Sci. Total Environ.*, 2018, **615**, 87–98.
2 H. Filik, A. A. Avan and E. K. Yetimoğlu, *Russ. J. Electrochem.*, 2019, **55**, 70–77.
3 Y. Yang, L. Lu, J. Zhang, Y. Yang, Y. Wu and B. Shao, *J. Chromatogr. A*, 2014, **1328**, 26–34.
4 J. R. Rochester and A. L. Bolden, *Environ. Health Perspect.*, 2015, **123**, 643–650.
5 A. Ullah, M. Pirzada, S. Jahan, H. Ullah, G. Shaheen, H. Rehman and M. A. Butt, *Chemosphere*, 2018, **209**, 508–516.

6 Z. Ye, Q. Wang, J. Qiao, B. Ye and G. Li, *J. Electroanal. Chem.*, 2019, **854**, 113541.
7 P. Dualde, O. Pardo, S. F. Fernández, A. Pastor and V. Yusà, *J. Chromatogr. B: Anal. Technol. Biomed. Life Sci.*, 2019, **1114**, 154–166.
8 K. Mandrah, G. N. V. Satyanarayana and S. K. Roy, *J. Chromatogr. A*, 2017, **1528**, 10–17.
9 Y. Zhang and X. Y. Chen, *Nanoscale*, 2019, **11**, 19105–19118.
10 J. J. Yang, J. T. Cao, H. Wang, Y. M. Liu and S. W. Ren, *Talanta*, 2017, **167**, 325–332.
11 L. Yang, W. Zhu, X. Ren, M. S. Khan, Y. Zhang, B. Du and Q. Wei, *Biosens. Bioelectron.*, 2017, **91**, 842–848.
12 D. J. E. Piper, G. J. Barbante, N. Brack, P. J. Pigram and C. F. Hogan, *Langmuir*, 2011, **27**, 474–480.
13 X. Cai, J. Yan, H. Chu, M. Wu and Y. Tu, *Sens. Actuators, B*, 2010, **143**, 655–659.
14 T. M. Downey and T. A. Nieman, *Anal. Chem.*, 1992, **64**, 261–268.
15 S. Bozorgzadeh, B. Haghighi and L. Gorton, *Electrochim. Acta*, 2015, **164**, 211–217.
16 C. Miao, B. Wu, H. Cao and N. Jia, *Anal. Methods*, 2014, **6**, 8592–8597.
17 X. Chen, S. Lian, Y. Ma, A. Peng, X. Tian and Z. Huang, *Talanta*, 2016, **146**, 844–850.
18 F. Shang, Y. Liu and S. Wang, *J. Electrochem. Soc.*, 2016, **163**, 280–285.
19 X. Li and X. Liu, *Nanoscale*, 2017, **9**, 7320–7341.
20 Y. Zhang, B. Ouyang, J. Xu, G. Jia, S. Chen, R. S. Rawat and H. J. Fan, *Angew. Chem.*, 2016, **128**, 8812–8816.
21 C. Ma, Y. Cao, X. Gou and J. J. Zhu, *Anal. Chem.*, 2020, **92**, 431–454.
22 D. W. M. Arrigan, *Analyst*, 2004, **129**, 1157–1165.
23 F. Xie, X. Cao, F. Qu, A. M. Asiri and X. Sun, *Sens. Actuators, B*, 2018, **55**, 1254–1261.
24 Z. Xue, J. Kang, D. Guo, C. Zhu, C. Li, X. Zhang and Y. Chen, *Electrochim. Acta*, 2018, **273**, 229–238.
25 N. Xiao, J. Deng, J. Cheng, S. Ju, H. Zhao, J. Xie, D. Qian and J. He, *Biosens. Bioelectron.*, 2016, **81**, 54–60.
26 C. Xie, H. Li, S. Li and J. Wu, *Anal. Chem.*, 2010, **82**, 241–249.
27 K. Kor and K. Zarei, *Talanta*, 2016, **146**, 181–187.
28 Y. T. Liu, J. Deng, X. L. Xiao, L. Ding, Y. L. Yuan, H. Li and L. L. Wang, *Electrochim. Acta*, 2011, **56**, 4595–4602.
29 H. Li, C. Xie and X. Fu, *Sens. Actuators, B*, 2013, **181**, 858–866.
30 B. Yang, J. Li and L. Zhang, *Analyst*, 2016, **141**, 5822–5828.
31 Y. Lin, J. Cao, X. Li, X. Zhang, J. Zhang and Z. Lin, *Anal. Methods*, 2016, **8**, 7445–7452.
32 M. L. Yola and N. Atar, *Ind. Eng. Chem. Res.*, 2017, **56**, 7631–7639.
33 B. Babamiri, A. Salimi, R. Hallaj and M. Hasanzadeh, *Biosens. Bioelectron.*, 2018, **107**, 272–279.
34 Y. Wang, D. Liu, Z. Liu, C. Xie, J. Huo and S. Wang, *Chem. Commun.*, 2016, **52**, 12614–12617.
35 J. Yin, Y. Li, F. Lv, Q. Fan, Y. Q. Zhao, Q. Zhang and S. Guo, *ACS Nano*, 2017, **11**, 2275–2283.
36 J. P. Sheng, L. Q. Wang, L. Deng, M. Zhang, H. C. He, K. Zeng, F. Y. Tang and Y. N. Liu, *ACS Appl. Mater. Interfaces*, 2018, **10**, 7191–7200.
37 R. Q. Li, P. Hu, M. Miao, Y. Li, X. F. Jiang, Q. Wu and X. B. Wang, *J. Mater. Chem. A*, 2018, **6**, 24767–24772.
38 J. P. Guin, M. Dinc and B. Mizaikoff, *ChemistrySelect*, 2018, **3**, 12223–12233.
39 P. Sikiti, T. A. Msagati, B. B. Mamba and A. K. Mishra, *J. Environ. Health Sci. Eng.*, 2014, **12**, 82.
40 H. Zeng, Y. Wang, X. Liu, J. Kong and C. Nie, *Talanta*, 2012, **93**, 172–181.
41 Y. Zhou, X. L. Ren, C. Sheng, X. Chen, Y. Kong, Y. Tao and Z. Chen, *J. Solid State Electrochem.*, 2012, **16**, 3159–3164.
42 F. shang, Y. Liu and S. Wang, *J. Electrochem. Soc.*, 2016, **163**, 280–285.
43 J. McCall, C. Alexander and M. M. Richter, *Anal. Chem.*, 1999, **71**, 2523–2527.
44 F. Li, Y. Pang, X. Lin and H. Cui, *Talanta*, 2003, **59**, 627–636.
45 W. Zheng, Z. Xiong, H. Li, S. Yu, G. Li and L. Niu, *Sens. Actuators, B*, 2018, **272**, 655–661.
46 H. S. Andersson, A. C. Koch-Schmidt, S. Ohlson and K. Mosbach, *J. Chromatogr. A*, 2010, **9**, 675–682.
47 N. B. Messaoud, A. A. Lahcen, C. Dridi and A. Amine, *Sens. Actuators, B*, 2018, **276**, 304–312.